One pair of motor neurons provokes early spontaneous motor behavior through periodic bursting in the chordate ascidian embryo

Taichi Akahoshi[a], Kouhei Oonuma[b], Makoto Murakami[b], Takeo Horie[c], Takehiro G. Kusakabe[b], Kotaro Oka[a] and Kohji Hotta[a 1]

[a] Department of Biosciences and Informatics, Faculty of Science and Technology, Keio University, Kohoku, Yokohama, 223-8522, Japan

[b] Institute for Integrative Neurobiology & Department of Biology, Konan University, Kobe, 658-8501, Japan

[c] Shimoda Marine Research Center, University of Tsukuba, Shimoda, Japan

1 To whom correspondence should be addressed. E-mail: khotta@bio.keio.ac.jp

Tel & Fax: +81-45-566-1700

Author Contributions: K.H. conceived this study; T.A., K.Ok., and K.H. designed the research; T.A. performed the research; K.H. and T.A. performed the dissociation experiment. K.Oo., M.M., T.H., T.G.K., and K.H. contributed reagents/analytic tools; K.Oo., M.M., and T.G.K. analyzed cell lineage; T.A. analyzed data; T.A. and K.H. wrote this manuscript and designed figures; K.Ok. and K.H. critically revised the manuscript and supervised the research.

Competing Interest Statement: The authors declare no conflict of interest.

Classification: BIOLOGICAL SCIENCES. Developmental Biology

Keywords: Ca^{2+} oscillation; cell lineage; motor neural circuit; pacemaker neuron; *Ciona*

This PDF file includes:

Main Text
Figures 1 to 4

Abstract

Swimming aquatic animals exhibit spontaneous motor behaviors before the maturation of swimming locomotion. In this study, we demonstrated that a single pair of motor neurons, A10.64/MN2, which exhibits periodic bursting, is essential for early spontaneous motor behaviors in the invertebrate chordate *Ciona intestinalis* type A (*Ciona robusta*). The Ca^{2+} oscillation was first observed only in a pair of cells at mid tailbud II (St.22) with an 80-sec interval, which shortened to 25 sec at late tailbud II (St.24). A dissociation experiment revealed that the Ca^{2+} oscillation occurred in a single cell independently. The start of the Ca^{2+} oscillation coincided with the Ca^{2+} elevation in ipsilateral tail muscle cells at late tailbud I (St.23). Cell lineage tracking

revealed that a pair of cells exhibiting Ca^{2+} oscillation corresponded to A10.64/MN2 motor neurons. Simultaneous imaging of Ca^{2+} and membrane potential demonstrated that the Ca^{2+} oscillation coupled with a burst firing of membrane potential. Interestingly, the number and frequency of tail muscle contractions initially coincided with those of the burst, but gradually came to coincide with those of spikes in the burst as the embryos developed toward late tailbud II (St.24). Finally, single-cell photoablation of A10.64/MN2 abolished early spontaneous motor behaviors until late tailbud II (St.24), suggesting that the early spontaneous motor behavior of *Ciona* is directly regulated by only a single pair of A10.64/MN2 motor neurons. These findings revealed that the chordate early spontaneous motor behavior was generated by a minimum motor circuit, consisting of a pair of motor neurons exhibiting periodic bursting.

Significance Statement

The ascidian provides insights into formation of chordate motor neural circuits that generate early spontaneous motor behavior. Whole-body Ca^{2+} imaging revealed that a pair of motor neurons exhibit spontaneous Ca^{2+} oscillation coinciding with Ca^{2+} elevation in tail muscle cells at a later stage. The cell lineage of the neuron exhibiting Ca^{2+} oscillation was identified as a motor neuron, A10.64/MN2. In this study, we emphasize that only one pair of motor neurons firstly exhibit rhythmic activity and directly triggers early spontaneous motor behavior. These findings markedly improve our understanding of the development of chordate motor neural circuits involved in early spontaneous motor behavior.

Main Text

Introduction

Swimming behavior is a common behavior observed in a variety of aquatic organisms. Before the maturation of swimming, embryos exhibit several stereotyped motor behaviors; in *Xenopus* and zebrafish, the earliest behaviors are spontaneous (1–3). Early spontaneous motor behaviors in vertebrates are driven by spontaneous network activity in the developing spinal cord (4, 5). However, little is known about the type of neurons that firstly becomes active in a motor neural circuit before the emergence of spontaneous network activity. A previous study (6) indicated that the motor neurons are activated first before the emergence of spontaneous network activity, whereas the interneurons are also active at the same time. Therefore, it remains unclear whether the motor neurons first become active independently or require interneuron activity.

The emergence of spontaneous network activity has been characterized by Ca^{2+} imaging as a transition from sporadic, cell-autonomous activity to coordinated rhythmic activity (6, 7). The significant characteristic of spontaneous motor behavior is its rhythmicity (8), and it is thought that pacemaker-like neurons trigger the early spontaneous motor behavior (9). In a study of zebrafish spinal cord, although motor neurons were activated first before the emergence of spontaneous network activity, ipsilateral caudal (IC) spinal interneurons were identified as the pacemaker-like neuron triggering spontaneous motor behavior (10). However, studies of chick and mouse suggested that cholinergic motor neurons are the first population of neurons responsible for triggering spontaneous motor activity (4, 5, 9). Thus, the pacemaker-like neurons that initially trigger the early spontaneous motor behavior have not been conclusively identified in the developing spinal cord (9).

In this study, we used the ascidian *Ciona intestinalis* type A to investigate formation of motor neural circuits involved in early spontaneous motor behavior before swimming locomotion. Although *Ciona* is the closest relative of vertebrates (11), its central nervous system (CNS) consists of only 177 neurons, and only five pairs of cholinergic motor neurons are present in the motor ganglion (12, 13). Furthermore, the CNS connectome of the tadpole larva was recently completed (13), and the cell lineage and expression profile of transcription factors in five pairs of motor neurons have been extensively investigated (12, 14–18). These advances allowed us to investigate which type of neurons firstly becomes active and trigger early spontaneous motor behavior in developing motor neural circuits of chordates.

Here, we show a single pair of motor neurons exhibits periodic bursting in the motor ganglion and triggers the early spontaneous motor behavior during chordate early embryogenesis.

Results

The Ca^{2+} oscillation is observed in a pair of cells and synchronizes with the activity of tail muscle cells in the tailbud embryos

We first examined the dynamics of intracellular Ca^{2+} transients in developing ascidian embryos using a genetically encoded Ca^{2+} indicator, GCamp6s (19). By injecting mRNA encoding GCaMP6s into unfertilized eggs, we could observe Ca^{2+} transients in the whole embryo from early gastrula (St.11) to late tailbud III (St.25) (20). As previously reported, the oscillation of Ca^{2+} transients (Ca^{2+} oscillation) was detected in the motor ganglion from the early- to mid- tailbud stage (Fig. 1A, 1B white arrowhead, and Movie S1), whereas no other reproducible Ca^{2+} transients were observed in any cells at this stage. The symmetric Ca^{2+} oscillation was detected on the left and right sides of the motor ganglion (Fig. 1D).

In mid tailbud II (St.22), the duration and interval of the Ca^{2+} oscillation in one side were 23 ± 4 (mean ± S.D.) sec and 80 ± 4 (mean ± S.D.) sec, respectively (Fig. 1B, 1C). The interval of Ca^{2+} oscillations varied at St.22, but gradually decreased to 25 sec toward late tailbud II (St.24) (Fig. 1E). The duration of Ca^{2+} oscillation also gradually decreased [12 ± 2 (mean ± S.D.) sec at St.23 and 10 ± 2 (mean ± S.D.) sec at St.24].

To determine how many cells are involved in the Ca^{2+} oscillation, the nucleus-localized Ca^{2+} sensor H2B-GCaMP6s was expressed throughout the embryo. Time-lapse imaging of the lateral side using confocal microscopy revealed that Ca^{2+} oscillation occurred only in a single nucleus (Fig. 1F and Movie S2), and no other cells exhibited reproducible Ca^{2+} transients at mid tailbud II (St.22). These observations indicated that the Ca^{2+} oscillation was derived from only a single pair of cells at mid tailbud II (St.22).

To determine whether a single cell has the potential to exhibit the Ca^{2+} oscillation independently, we dissociated tailbud embryo expressing GCaMP6s to single cells and observed the Ca^{2+} elevation (Fig. 1G and Movie S3). Surprisingly, time-lapse imaging revealed a cell-autonomous Ca^{2+} oscillation at an interval of 40–80 sec (Fig. 1H). Thus, the Ca^{2+} oscillation during the tailbud stage was caused by a single cell independently, without any contribution from other cells.

Continuous whole-embryo Ca^{2+} imaging revealed that the Ca^{2+} oscillation began at the same time as the Ca^{2+} elevation in the ipsilateral tail muscle from late tailbud I (St.23) (Fig. 1I 202 sec, 1J blue box). Tail muscle contraction was also observed as a movement of the tail when the Ca^{2+} elevation occurred (Movie S4, approximately 7 min). Ca^{2+} oscillations in the motor ganglion sometimes did not synchronize with the Ca^{2+} elevation in the tail muscle (Fig. 1J asterisk), but fully synchronized 10 min after the first synchronization. These results suggest that the pair of cells exhibiting Ca^{2+} oscillation is one of the motor neurons, and that these cells regulate the activity of tail muscle from late tailbud I (St.23).

A motor neuron, MN2/A10.64, causes cell-autonomous Ca^{2+} oscillation

Because the region of fluorescence of Ca^{2+} oscillation was relatively large and located in the motor ganglion (Fig. 1B), we expected that the pair of cells exhibiting Ca^{2+} oscillation corresponded to motor neurons derived from A10.64 (Fig. 1A). A10.64 is the largest motor neuron, located bilaterally in the motor ganglion at mid tailbud II (13, 21, 22).

To test this hypothesis, we investigated the cell lineage of a pair of cells exhibiting Ca^{2+} oscillation. We simultaneously induced Neurog::Kaede-NLS and pSP-CiVACHT::GCaMP6s. Neurog::Kaede-NLS was expressed exclusively in the nuclei of A9.31 and A9.32 (mother cell of A10.64) at late gastrula (St.13) (23) (Fig. 2A and 2B). pSP-CiVACHT::GCaMP6s is expressed in the cytoplasm of pan-cholinergic motor neurons (24).

Time-lapse recording starting in late gastrula revealed that A9.32 divided at mid neurula, and that A10.64 then migrated anteriorly along the neural tube (Fig. 2C), as reported previously (17). As a result, a pair of Kaede nucleus-localized signal of A10.64 appeared exclusively in the motor ganglion at late tailbud I (St.23) (Fig. 2C, 137 min). Finally, we confirmed that the Ca^{2+} oscillation

in the cytoplasm was overlapped with the Kaede nucleus-localized signal of A10.64 (Fig. 2D yellow arrowhead, Movie S5). Based on these findings, we identified the cells exhibiting Ca^{2+} oscillation as A10.64, one of the cholinergic motor neurons named MN2 (13).

Tail muscle contraction gradually changes the coupling partner, from the individual bursts to the individual spikes of A10.64, during development

Because the Ca^{2+} oscillation occurred in a pair of cholinergic motor neurons, A10.64/MN2, we speculated that the Ca^{2+} oscillation occurred as a result of neuronal activity. To understand the relationships between Ca^{2+} oscillation and membrane potential, we first tried simultaneous recordings of Ca^{2+} and membrane potential using the red fluorescent Ca^{2+} indicator NES-jRGECO1a (25) and the voltage sensor ASAP2f (26). The antagonist of nicotinic acetylcholine receptor, D-tubocurarine, was used to inhibit larval motility for the recordings of membrane potential. In the Ca^{2+} transient (Fig. 3A and Fig. S1, red graph), we could observe burst firing of membrane potential in A10.64 (Fig. 3A and Fig. S1, green graph). Each burst consisted of multiple spikes (Fig. 3A and Fig. S1, asterisks). Because every burst was accompanied by a single Ca^{2+} transient, the timing and interval of the bursts were consistent with those of the Ca^{2+} oscillations (Fig. 1E).

The average number of spikes in a burst was 6.3 ± 5.4 at late tailbud I (St.23), decreasing significantly to 2.6 ± 1.4 at late tailbud II (St.24) ($p<0.05$) (Fig. 3B). The inter-spike interval in a burst was 0.5 ± 0.3 sec at late tailbud I (St.23), decreasing significantly to 0.2 ± 0.04 sec at late tailbud II (St.24) ($p<0.05$) (Fig. 3C). D-tubocurarine affected neither the number of spikes in the burst nor the inter-spike interval (ISI) in the embryos at St.23 (Fig. 3B, C).

Tail muscle contraction was first observed as movement of the tail in St.23, when Ca^{2+} elevation occurred in the tail muscle (Movie S4). Although the swimming behavior of *Ciona* has been characterized in matured larvae, both behaviorally and electrophysiologically (27–30), the behavior of embryos before hatching is relatively uncharacterized, with only a few mentions (31). Therefore, we next characterized the behavior of embryos at St.23 and St.24 and compared them with the burst firing of membrane potential in A10.64. We used a high-speed camera to record the behavior, and found that muscle contractions occurred on the left and right sides, respectively, in St.23 and St.24 (Fig. 3D and 3E). However, the interval between left and right muscle contraction was several seconds, much longer than that of swimming behavior in hatched larvae, in which the interval between left and right muscle contraction is 15–25 msec (27). Accordingly, we referred each unilateral muscle contraction as an “early tail-flick” (ETF). The averaged interval of the ETF was 79 ± 14 (mean ± S.D.) sec at St.23, decreasing to 21 ± 6 (mean ± S.D.) sec at St.24, comparable to the change in the Ca^{2+} oscillation in A10.64 from St.23 to St.24 (80 sec to 25 sec; Fig. 1E). Interestingly, tail muscle contraction occurred only once in one ETF at St.23, whereas two or three consecutive muscle contractions occurred in one ETF at St.24 (Fig. 3E). The number and frequency of tail muscle contractions in one ETF at St.24 (Fig. 3E, F) were comparable to those of spikes in the burst at St.24 (Fig. 3B and C). These observations indicated that muscle contraction in one ETF gradually coupled to the individual spike in the burst of A10.64 as the embryo developed toward St.24.

Single-cell photoablation for A10.64 abrogates the ETF until St.24

Because the number and frequency of muscle contractions in one ETF at late tailbud II (St.24) were comparable to those of spikes in the burst of A10.64 at St.24, we hypothesized that the neuronal activity of the A10.64 would be sufficient to regulate the ipsilateral ETF at least until St.24. To test this idea, we attempted single-cell photoablation for A10.64 using an LOV-based optogenetic tool, miniSOG2, which produces singlet oxygen by laser irradiation (32). We targeted the mCherry-CAAX signal of A10.64 and expected that penetration of the laser would completely suppress the ETF (Fig. 4A, 4B).

In contrast to the control embryo (electroporated only with Neurog::mCherry-CAAX), the embryo expressing miniSOG2 did not exhibit ETF at St.24 (Fig. 4C and 4D). In the absence of 440-nm laser irradiation, early motor behavior was comparable to that in the control embryos (Fig. S2).

Together, these results suggested that oscillatory neuronal activity of a single pair of cells, A10.64, directly regulates the ETF until St.24. Although single-cell photoablation of A10.64

abolished early spontaneous motor behavior until St.24, tail muscle contraction recovered at a later stage (Movie S6). This observation suggests that another type of motor neuron starts to be active later and forms a neuromuscular junction after St.24 (33).

Discussion

Neuronal activity of A10.64 is essential for the early spontaneous motor behavior

In this study, we found that a single pair of motor neurons, A10.64, exhibits Ca^{2+} oscillation in St.22 (Fig. 2D), and that A10.64 independently oscillates (Fig. 1G, H). Furthermore, we revealed the relationship between the Ca^{2+} oscillation, the burst firing of membrane potential, and the early spontaneous motor behavior until St.24. Based on our results, early development of the motor neural circuit proceeds as follows (Fig. 4E).

1. From early to mid tailbud II (St.20 to St.22), Ca^{2+} oscillation first occurs only in A10.64 (Fig. 1D). The interval and the duration of the Ca^{2+} oscillation are 80 sec and 23 sec, respectively (Fig. 1E). Ca^{2+} oscillation couples with the burst firing of membrane potential. No muscle contraction is observed in this stage.
2. In the late tailbud I (St.23), Ca^{2+} oscillation in A10.64 first coincides with the Ca^{2+} elevation of ipsilateral tail muscle (ETF), suggesting the formation of neuromuscular junctions (Fig. 4E, yellow stars). The interval and duration of each Ca^{2+} transient both get shorter. Tail muscle contraction occurs, but only once per burst.
3. In late tailbud II (St.24), both the interval and duration of each Ca^{2+} transient are shorter, approaching 25 sec and 10 sec, respectively. The number and frequency of muscle contraction in the ETF coincide with those of spikes in the burst, such that two or three consecutive tail muscle contractions occur in one burst of A10.64.

In this manner, the early spontaneous motor behavior of *Ciona* is gradually fine-tuned to the oscillatory neuronal activity of A10.64. After St.24, embryos gradually develop left–right alternative muscle contraction by adding reciprocal connection by anterior caudal inhibitory neurons (ACINs) to motor circuit (34), leading to the swimming locomotion of hatched larvae (St.26) (27). What, then, is the function of A10.64 in motor behavior after St.24?
It is possible that A10.64 continues to play a central role of the motor circuit at later stages, for the following reason. In the larval stage, 12 pairs of neurons and a single neuron are located in the motor ganglion (13). All five pairs of motor neurons, including A10.64, were sustained to the mature larva (13). It has been proposed that a neural circuit comprising five pairs of motor neurons and ACINs is responsible for generation of left–right alternative motor behavior in the adult larva (12). ACINs extend the axon anteriorly and are connected to the contralateral motor neurons (13). Furthermore, ACINs are identified GABAergic/glycinergic neurons (34), and knockdown of glycine receptor disrupts alternating swimming behavior (35). These results indicate that ACINs are candidates for the reciprocal inhibitory system that generates swimming locomotion (12). In this study, we found that neuronal activity of A10.64 triggers ETF until St.24. It is possible that A10.64 could trigger left–right alternative muscle contraction through periodic bursting as a component of the reciprocal inhibitory system at St.26. Supporting this, the interval of swimming behavior of decereberated larvae was approximately 20 sec (Nishino et al., personal communication; in prep.), consistent with the interval of the Ca^{2+} oscillation in A10.64 at St.24 (Fig. 1E).

Evolutionarily conserved characteristics between A10.64 and the first active motor neuron of vertebrates

Among five pairs of cholinergic motor neurons, A10.64 is the only neuron that expresses the homeobox gene, *islet* (36). *islet* is the earliest marker of developing motor neurons (37) and is required for the specification and maintenance of spinal motor neurons (38). Interestingly, in the zebrafish spinal cord, *islet*-positive motor neurons are active before the emergence of spontaneous network activity. Later, these neurons form local patterned activity with neighboring

neurons and ultimately orchestrate the left–right alternative patterns called coiling (6). The similarity of marker gene expression, and characteristic that firstly become active in the developing motor circuit, with the zebrafish spinal motor neurons, it is possible that A10.64 is the first active neuron that triggers spontaneous left–right alternative motor behavior at later stages in chordates.

The mechanism of Ca^{2+} oscillation

In vertebrates, it has been hypothesized that periodic bursting in motor neurons occurs through electrical coupling with other neurons exhibiting periodic depolarization. In the zebrafish spinal cord, motor neurons exhibit periodic depolarization through electrical coupling with ipsilateral caudal (IC) spinal interneurons, which have been proposed to act as pacemaker-like neurons, triggering spontaneous motor behavior (10, 39). However, in this study, no other Ca^{2+} activity coupled with the Ca^{2+} oscillation of A10.64 at St.22 (Fig. 1F and Movie S2). The dissociation experiment clearly showed that the Ca^{2+} oscillation occurred independently in a single cell (Fig. 2E), meaning that Ca^{2+} oscillation occurs endogenously; thus, A10.64 may act as a pacemaker-like neuron. Evolutionary point of view, it is interesting whether the role of motor neuron is commonly possessed from chordate ancestor or only in ascidian characteristics after the divergence of ascidian lineage.

In general, pacemaker-like neurons exhibit oscillatory depolarization and hyperpolarization (9). Depolarization can be caused by channels such as persistent sodium channels (40, 41) or hyperpolarization-activated cation channels (I_h current) (42). Hyperpolarization is typically caused by the Ca^{2+}-activated K^+ current (43). Conducting scRNA-seq of A10.64 will identify the channel molecules responsible for periodic bursting in this pair of neurons.

Materials and Methods

Experimental Animals

Ciona robusta (*Ciona intestinalis* type A) adults were obtained from Maizuru Fisheries Research Station (Kyoto University), Onagawa Field Center (Tohoku University), and Misaki Marine Biological Station (The University of Tokyo) through the National Bio-Resource Project (NBRP), Japan. Eggs and sperm were collected by dissection of oviducts and sperm ducts, respectively. After artificial insemination, fertilized eggs were incubated at 15–20°C until observation.

Preparation of reporter constructs and gene transduction

pGP-CMV::GCaMP6s (19), pGP-CMV::NES-jRGECO1a (25), ASAP2f (26), and pcDNA3.1::miniSOG2-T2A-H2B-EGFP (32) were purchased from Addgene (USA). pSP-CiVACHT::Kaede was purchased from *Ciona intestinalis* Transgenic line RESources (CITRES). Neurog::Kaede-NLS was made as follows: a 3.6-kb upstream region of the *Ciona neurogenin* gene (*Neurog*) was amplified by PCR using a pair of primers (forward primer, AGGGATCCGGAAGAGGTGTTAGA; reverse primer, GGGGATCCATTTTGTAGCAAGAGC) and cloned into the pSP-Kaede-NLS vector (44).

pSP-Neurog::Kaede, which was used for immunostaining of Kaede at late gastrula, was made as follows: a 3.6-kb upstream region of the *Ciona neurogenin* gene (*Neurog*) was subcloned into the BamHI restriction site of the pSP-Kaede vector.

For micro-injection, mRNA encoding GCaMP6s was synthesized from pSPE3::GCaMp6s as previously described (20). For synthesis of mRNA encoding H2B-GCaMP6s, the ORF of H2B was PCR-amplified from Foxb::H2B-CFP (forward primer, TCTGAATTCAGGCCTATGGTTGCATCCAAA; reverse primer, GGCGACTGGTGGATCTTTTGAGCTGGTGTA), and GCaMP6s was PCR-amplified from pSPE3::GCaMp6s (forward primer, GATCCACCAGTCGCCACCATGGGTTCTCAT; reverse primer, AGGCCTGAATTCAGATCTGCCAAAGTTGAG). The cloning reaction for pSPE3::H2B-GCaMp6s was performed using linearized PCR products and the In-Fusion HD Cloning Kit (Takara Bio). H2B-GCaMP6s mRNA was produced and precipitated using the mMESSAGE

mMACHINE T3 kit (Life Technologies, Carlsbad, CA, USA). GCaMP6s or H2B-GCAMP6s mRNA was injected into dechorionated eggs at 0.5 µg/µl.
For electroporation, pSP-CiVACHT::GCaMP6s, pSP-Neurog::ASAP2f, pSP-Neurog::NES-jRGECO1a, pSP-Neurog::minisog2-CAAX, and pSP-Neurog::mCherry-CAAX were synthesized as described for pSPE3::H2B-GCaMp6s. Forty microliters of each plasmid construct at 1000 ng/µl was combined with the 360 µl of 0.77 M mannitol in 10% seawater. At 30 min post-fertilization, eggs in 400 µl of this solution were placed in a cuvette for electroporation. After electroporation, eggs were washed with seawater and incubated until observation. For membrane potential imaging, embryos at St.23 and St.24 were paralyzed with 5 mM D-tubocurarine 30 min before observation, as tail muscle contraction prevents measurement of membrane potential (45).

Immunostaining of late gastrula embryo with Kaede antibody and DAPI
Immunofluorescence staining was carried out as described previously (46). To visualize the localization of fluorescent reporter proteins, rabbit anti-Kaede polyclonal (PM012; Medical & Biological Laboratories, Nagoya, Japan; for Kaede) was used as the primary antibody (diluted 1:1000). The secondary antibody was Alexa Fluor 594–conjugated anti-rabbit IgG (A11012; Thermo Fisher Scientific). Samples were mounted under a coverslip in 50% glycerol-PBST with mounting Medium with DAPI (Vector Laboratories).

Microscopy
The embryos were observed by fluorescence microscopy with a 3CCD (C7800-20, Hamamatsu Photonics) camera or by confocal laser-scanning microscopy (CLSM). A Nikon inverted microscope (Nikon eclipse, IX71) with a 20× or 40× objective lens (LUCPlanFLN) was used for fluorescence imaging with a U-MWBV2 mirror unit (Olympus). A SOLA LED light (Lumencor) was used as the light source, and fluorescence images were acquired with a 3CCD camera and the AQUACOSMOS software (Hamamatsu Photonics). For Ca^{2+} imaging, the time interval was set to 1–5 sec per frame. For membrane potential imaging, the time interval was set to 20 msec per frame.
For CLSM imaging, an Olympus fv1000 microscope was used. Excitation was at 488 nm to visualize the signals of GCaMP6s and Kaede, and at 559 nm to visualize the signal of mCherry. An Olympus 20× or 40× oil immersion lens was used.

Fluorescence image analysis
Fluorescence intensities in image data were analyzed using the AQUACOSMOS software. Numerical data were exported into Microsoft Office Excel 2016 (Microsoft, Redmond, WA, USA) for graph plotting. Statistical analyses were performed in R (CRAN).

Cell lineage tracking
The Z-stack images of the dorsal side of late gastrula embryos electroplated with Neurog::Kaede-NLS and pSP-CiVACHT::GCaMP6s were acquired every 10 min until late tailbud I (St.23) using an Olympus fv1000 microscope. The photo-conversion of Kaede was performed by executing bleaching with SIM scanner by manual operation. The Kaede signal of a pair of A9.32 cells at late gastrula (St.13) was photo-converted by irradiation with a 405-nm laser for a few seconds.

Single-cell photoablation of A10.64
Single-cell photoablation of A10.64 was performed using miniSOG2, which produces singlet oxygen by laser stimulation. pSP-Neurog::minisog2-CAAX is used to express miniSOG2 at A10.64 and pSP-Neurog::mCherry-CAAX is used to label the A10.64 for laser stimulation.
In the mid tailbud II (St.22), mCherry-CAAX was expressed exclusively in A10.64 (Fig. 4B). The embryos (St.22) electroplated with pSP-Neurog::minisog2-CAAX and pSP-Neurog::mCherry-CAAX were ablated from the lateral side by irradiation with a laser (440 nm: 15 µW/cm^2) for 10 min (Fig. 4A).
For the control, embryos electroporated with pSP-Neurog::mCherry-CAAX were ablated from the lateral side by irradiation with a laser (440 nm: 15 µW/cm^2) for 10 min (Fig. 4A). The ROI (region of interest) for laser stimulation was set to the region of fluorescence by mCherry. The ablation

was performed once per minute to correct the position of the ROI. After laser irradiation, the behavior of embryos were recorded using a high-speed camera (WRAYCAM-VEX230M, WRAYMER, Osaka, Japan) attached to a stereoscopic microscope (OLYMPUS, SZX12, Tokyo, Japan) for 2 min by every 30 min. Optical images were captured at 200–500 fps to quantify the temporal change of curvature for the early spontaneous motor behavior.

Quantification of the ETF

To quantify early spontaneous motor behavior, recording data were processed using the open-source program Fiji (National Institutes of Health, Bethesda, MD, USA) and MATLAB (MathWorks). The binarization and skeletonization (47) of the images were processed by Fiji, and then skeleton pruning was processed using a custom-made MATLAB script (MathWorks). The midline of the embryos at each time point was extracted, and the curvature of the midline was calculated using the position of three points on the midline: start, (A), mid (B), and end (C). The equation of the calculation of curvature is as follows.

$$curv. = \frac{1}{R} = \frac{2sin\,C}{C} = \frac{2}{|\overrightarrow{A-B}|}\frac{(\overrightarrow{A-C})\times(\overrightarrow{B-C})}{|\overrightarrow{A-C}||\overrightarrow{B-C}|}$$

Acknowledgments

Ciona intestinalis type A was provided by Dr. Yutaka Satou at Kyoto University and Dr. Manabu Yoshida at The University of Tokyo with support by the National Bio-Resource Project of AMED, Japan. Valuable discussion and comments were provided by Shuya Hasegawa and Atsuo S. Nishino (Hirosaki University).

This work was supported by JSPS KAKENHI Grants JP16H01451 and JP16K07426 (to K.H.), 19J21665 (to T.A.), 19H03213 (to T.G.K.), 17K15130 (to K.Oo.) and 19H03204 (to T.H.). K.H. is also supported by Keio Gijuku Academic Development Funds. T.H. is also supported by Toray Science and Technology Grant, Takeda Science Foundation and Mochida Memorial Foundation for Medical and Pharmaceutical Research. K.Oo. is also supported by a Sasakawa Scientific Research Grant from The Japan Science Society.

References

1. L. Muntz, Myogenesis in the trunk and leg during development of the tadpole of Xenopus laevis (Daudin 1802). *J. Embryol. Exp. Morphol.* **33**, 757–774 (1975).
2. L. Saint-Amant, P. Drapeau, Time course of the development of motor behaviors in the zebrafish embryo. *J. Neurobiol.* **37**, 622–632 (1998).
3. P. van Mier, J. Armstrong, A. Roberts, Development of early swimming inXenopus laevis embryos: Myotomal musculature, its innervation and activation. *Neuroscience* **32**, 113–126 (1989).).
4. M. Gartz Hanson, L. T. Landmesser, M. G. Hanson, L. T. Landmesser, Characterization of the circuits that generate spontaneous episodes of activity in the early embryonic mouse spinal cord. *J. Neurosci.* **23**, 587–600 (2003).
5. P. Wenner, M. J. O'Donovan, Mechanisms that initiate spontaneous network activity in the developing chick spinal cord. *J. Neurophysiol.* **86**, 1481–1498 (2001).
6. Y. Wan, *et al.*, Single-Cell Reconstruction of Emerging Population Activity in an Entire Developing Circuit. *Cell* **179**, 355--372.e23 (2019).
7. E. Warp, *et al.*, Emergence of Patterned Activity in the Developing Zebrafish Spinal Cord. *Curr. Biol.* **22**, 93–102 (2012).
8. V. Hamburger, "Some Aspects of the Embryology of Behavior" (1963).
9. A. G. Blankenship, M. B. Feller, Mechanisms underlying spontaneous patterned activity in developing neural circuits. *Nat. Rev. Neurosci.* **11**, 18–29 (2010).
10. H. Tong, J. R. McDearmid, Pacemaker and Plateau Potentials Shape Output of a Developing Locomotor Network. *Curr. Biol.* **22**, 2285–2293 (2012).

11. N. Satoh, D. Rokhsar, T. Nishikawa, Chordate evolution and the three-phylum system. *Proc. R. Soc. B Biol. Sci.* **281**, 20141729 (2014)..
12. T. Horie, M. Nakagawa, Y. Sasakura, T. G. Kusakabe, Cell type and function of neurons in the ascidian nervous system. *Dev. Growth Differ.* **51**, 207–220 (2009).
13. K. Ryan, Z. Lu, I. A. Meinertzhagen, The CNS connectome of a tadpole larva of Ciona intestinalis (L.) highlights sidedness in the brain of a chordate sibling. *Elife* **5**, e16962 (2016).
14. E. K. Lowe, A. Stolfi, Developmental system drift in motor ganglion patterning between distantly related tunicates. *Evodevo* **9**, 18 (2018).
15. A. Stolfi, M. Levine, Neuronal subtype specification in the spinal cord of a protovertebrate. *Development* **138**, 995–1004 (2011).
16. C. Hudson, M. Ba, C. Rouviere, H. Yasuo, Divergent mechanisms specify chordate motoneurons: evidence from ascidians. *Development* **138**, 1643–1652 (2011).
17. I. A. Navarrete, M. Levine, Nodal and FGF coordinate ascidian neural tube morphogenesis. *Dev.* **143**, 4665–4675 (2016).
18. A. Stolfi, E. Wagner, J. M. Taliaferro, S. Chou, M. Levine, Neural tube patterning by Ephrin, FGF and Notch signaling relays. *Development* **138**, 5429–5439 (2011).
19. T. W. Chen, *et al.*, Ultrasensitive fluorescent proteins for imaging neuronal activity. *Nature* **499**, 295–300 (2013).
20. T. Akahoshi, K. Hotta, K. Oka, Characterization of calcium transients during early embryogenesis in ascidians Ciona robusta (Ciona intestinalis type A) and Ciona savignyi. *Dev. Biol.* **431**, 205–214 (2017).
21. A. G. Cole, I. A. Meinertzhagen, The central nervous system of the ascidian larva: Mitotic history of cells forming the neural tube in late embryonic Ciona intestinalis. *Dev. Biol.* **271**, 239–262 (2004).
22. M. J. Nakamura, J. Terai, R. Okubo, K. Hotta, K. Oka, Three-dimensional anatomy of the Ciona intestinalis tailbud embryo at single-cell resolution. *Dev. Biol.* **372**, 274–284 (2012).
23. K. S. Imai, A. Stolfi, M. Levine, Y. Satou, Gene regulatory networks underlying the compartmentalization of the Ciona central nervous system. *Development* **136**, 285–293 (2009).
24. T. Horie, *et al.*, Ependymal cells of chordate larvae are stem-like cells that form the adult nervous system. *Nature* **469**, 525–529 (2011).
25. H. Dana, *et al.*, Sensitive red protein calcium indicators for imaging neural activity. *Elife* **5**, 1–24 (2016).
26. H. H. Yang, et al., Subcellular Imaging of Voltage and Calcium Signals Reveals Neural Processing In Vivo. *Cell* **166**, 245–257 (2016).
27. G. Zega, M. C. Thorndyke, E. R. Brown, Development of swimming behaviour in the larva of the ascidian Ciona intestinalis. *J. Exp. Biol.* **209**, 3405–3412 (2006).
28. J. Rudolf, D. Dondorp, L. Canon, S. Tieo, M. Chatzigeorgiou, Automated behavioural analysis reveals the basic behavioural repertoire of the urochordate Ciona intestinalis. *Sci. Rep.* **9**, 2416 (2019).
29. M. Nakagawa, T. Miyamoto, M. Ohkuma, M. Tsuda, Action spectrum for the photophobic response of Ciona intestinalis (Ascidieacea, Urochordata) larvae implicates retinal protein. *Photochem. Photobiol.* **70**, 359–362 (1999).
30. M. Tsuda, D. Sakurai, M. Goda, Direct evidence for the role of pigment cells in the brain of ascidian larvae by laser ablation. *J. Exp. Biol.* **206**, 1409–1417 (2003).
31. Q. Bone, On the locomotion of ascidian tadpole larvae. *J. Mar. Biol. Assoc. United Kingdom* **72**, 161–186 (1992).
32. K. Makhijani, *et al.*, Precision Optogenetic Tool for Selective Single- and Multiple-Cell Ablation in a Live Animal Model System. *Cell Chem. Biol.* **24**, 110–119 (2017).
33. N. Okawa, et al., Cellular identity and Ca2+ signaling activity of the non-reproductive GnRH system in the Ciona intestinalis type A (Ciona robusta) larva. *Sci. Rep*. **10**, 18590 (2020).

34. T. Horie, M. Nakagawa, Y. Sasakura, T. G. Kusakabe, M. Tsuda, Simple motor system of the ascidian larva: Neuronal complex comprising putative cholinergic and GABAergic/Glycinergic neurons. *Zoolog. Sci.* **27**, 181–190 (2010).
35. A. Nishino, Y. Okamura, S. Piscopo, E. R. Brown, A glycine receptor is involved in the organization of swimming movements in an invertebrate chordate. *BMC Neurosci.* **11**, 6 (2010).
36. C. Hudson, The central nervous system of ascidian larvae. Wiley Interdiscip. *Rev. Dev. Biol.* **5**, 538-561 (2016).
37. J. Ericson, S. Thor, T. Edlund, T. Jessell, T. Yamada, Early stages of motor neuron differentiation revealed by expression of homeobox gene Islet-1. *Science* **256**, 1555-1560 (1992).
38. X. Liang, *et al.*, Isl1 Is required for multiple aspects of motor neuron development. *Mol. Cell. Neurosci.* **47**, 215–222 (2011).
39. L. Saint-Amant, P. Drapeau, Motoneuron activity patterns related to the earliest behavior of the zebrafish embryo. *J. Neurosci.* **20**, 3964–3972 (2000).
40. J. F. R. Paton, A. P. L. Abdala, H. Koizumi, J. C. Smith, W. M. St-John, Respiratory rhythm generation during gasping depends on persistent sodium current. *Nat. Neurosci.* **9**, 311–313 (2006).
41. M. Le Bon-Jego, R. Yuste, Persistently Active, Pacemaker-Like Neurons in Neocortex. *Front. Neurosci.* **1**, 123–129 (2007).
42. M. Biel, C. Wahl-Schott, S. Michalakis, X. Zong, Hyperpolarization-activated cation channels: From genes to function. *Physiol. Rev.* **89**, 847–885 (2009).
43. D. Weisbrod, *et al.*, SK4 Ca2+ activated K+ channel is a critical player in cardiac pacemaker derived from human embryonic stem cells. *Proc. Natl. Acad. Sci. U. S. A.* **110** (2013).
44. K. Oonuma, *et al.*, Revised lineage of larval photoreceptor cells in Ciona reveals archetypal collaboration between neural tube and neural crest in sensory organ formation. *Dev. Biol.* **420**, 178–185 (2016).
45. Y. Ohtsuka, Y. Okamura, Voltage-dependent calcium influx mediates maturation of myofibril arrangement in ascidian larval muscle. *Dev. Biol.* **301**, 361–373 (2007).
46. K. Nishitsuji, *et al.*, Cell lineage and cis-regulation for a unique GABAergic/glycinergic neuron type in the larval nerve cord of the ascidian Ciona intestinalis. *Dev. Growth Differ.* **54**, 177–186 (2012).
47. T. Y. Zhang, C. Y. Suen, A Fast Parallel Algorithm for Thinning Digital Patterns. *Commun. ACM* **27**, 236–239 (1984).

Figures and Tables

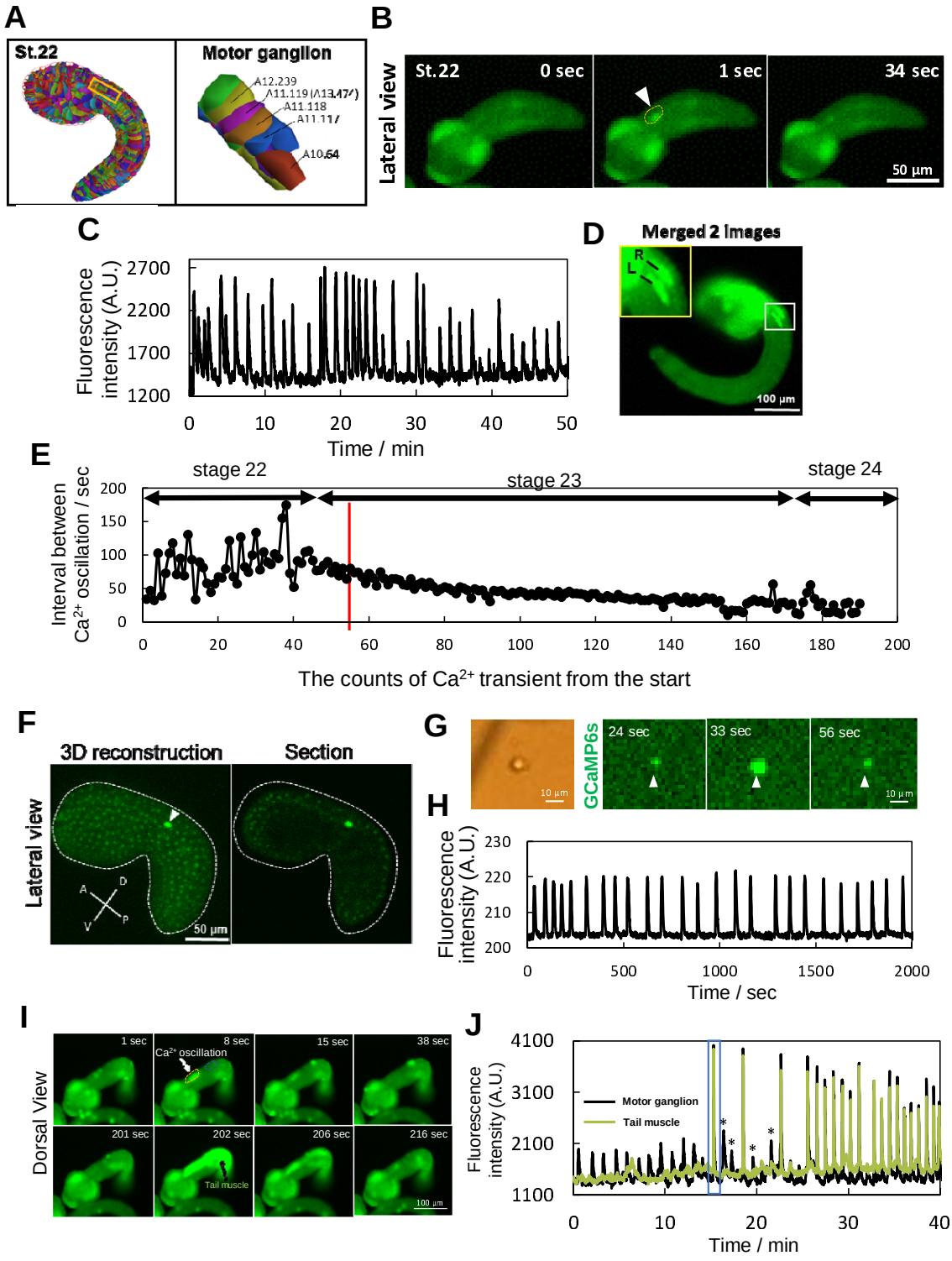

Figure 1. Ca^{2+} oscillation was observed in a pair of cells and synchronized with the activity of tail muscle cells at the tailbud stage.

(A) 3D reconstruction of a *Ciona* embryo at mid tailbud II (St.22), modified from (22). The region of the motor ganglion (yellow rectangle) is magnified in the right panel. The cell lineage of five pairs of cholinergic motor neurons was indicated. A11.119 is the mother cell of the motor neuron A13.474. (B) The representative time course image of the Ca^{2+} transient in the motor ganglion at St.22. Ca^{2+} transient is indicated by a white arrowhead (second panel). (C) Fluorescence intensity of Ca^{2+} in the ROI (region of interest, Fig.1B, yellow dotted line) overtime for 50 min. (D) Merged images of Ca^{2+} imaging at different time points. Ca^{2+} transients were observed on the left and right sides of the motor ganglion, respectively (yellow box; enlarged view of the white box, inset). R, right; L, left (E) Transition of the interval between Ca^{2+} oscillations over time. As the count of Ca^{2+} transients increases, the interval between Ca^{2+} oscillations gradually decreases. Red line indicates the time when Ca^{2+} oscillations first coincided with the Ca^{2+} elevation of the ipsilateral muscle. Approximate developmental stage is indicated. (F) 3D reconstruction (left panel) and section (right panel) images of the Ca^{2+} oscillation by H2B-GCaMP6s. Ca^{2+} oscillation is indicated by the white arrowhead. Ca^{2+} oscillation occurs only in a single nucleus. A, anterior; D, dorsal; P, posterior; V, ventral. (G) Image of a dissociated single cell and time-course images of Ca^{2+} oscillation in the same cell. N=6. (H) Change in the fluorescence intensity of Ca^{2+} in (G) over 2000 sec. (I) Representative time-course image of Ca^{2+} oscillation at St.23. After a few minutes, the Ca^{2+} oscillation (white arrow, 8 sec) coincides with the Ca^{2+} elevation in the ipsilateral muscle cells (black arrow, 202 sec). (J) Fluorescence intensity over time in the motor ganglion and tail muscle at St.23. ROI (region of interest) was set in (Fig.1I 8 sec, yellow dotted line for motor ganglion, blue dotted line for tail muscle cell). The time when the Ca^{2+} oscillation and Ca^{2+} elevation of ipsilateral muscle cells first coincided is indicated by a blue rectangle. The asterisks indicate Ca^{2+} oscillation without synchronization of the Ca^{2+} elevation in ipsilateral muscle cells after the first synchronization.

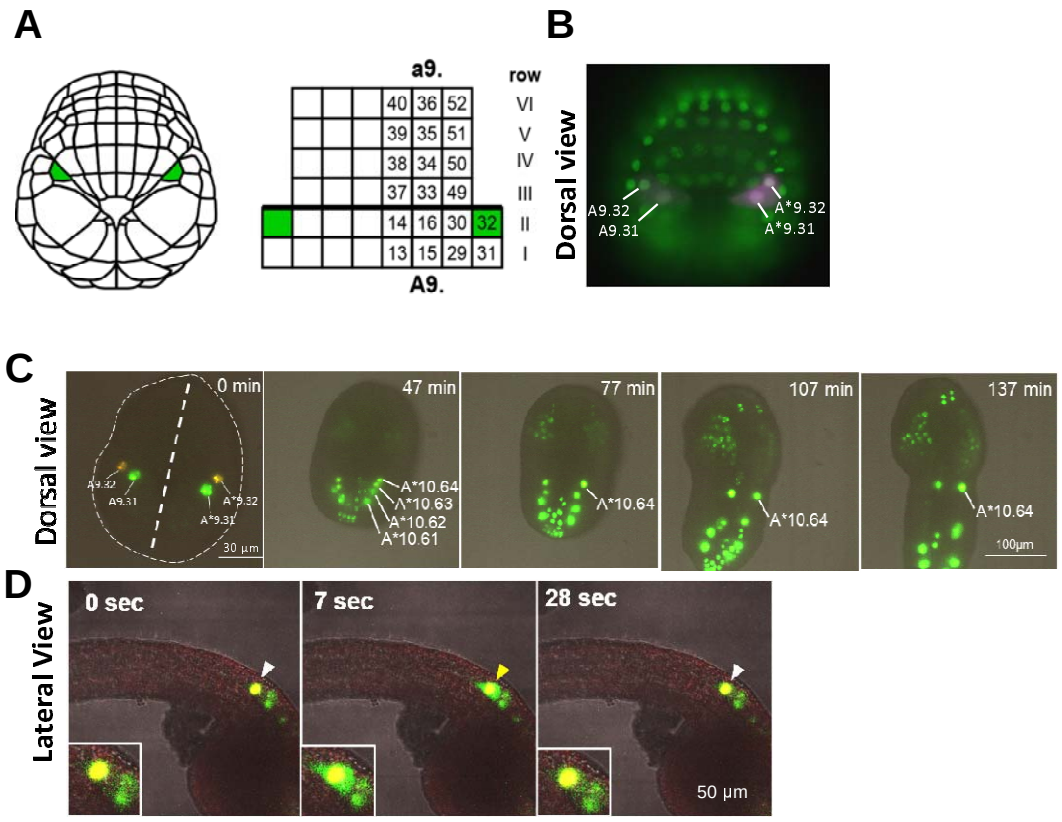

Figure 2. The motor neuron MN2/A10.64 causes cell-autonomous Ca^{2+} oscillation.
(A) Schematic illustrations of the late gastrula (St.13) (left) and the cell lineage of the neural plate cells (right). A9.32 cells are indicated in green. (B) Late gastrula embryo expressing Kaede under the control of the Neurogenin promoter. Kaede was immunostained with antibodies (magenta). Nuclei are stained with DAPI (green). Compared with Fig. 2A, A9.32 and A9.31 cells are identified. A9.32 and A9.31 cells overlapped with immunostained signals from Kaede. (C) Cell lineage tracking of A9.32 cells from late gastrula (St.13) to late tailbud I (St.23). The embryo was electroporated with Neurog::Kaede-NLS and pSP-CiVACHT::GCaMP6s. The sister cell of the A9.32, A10.64, migrates anteriorly and is localized to the motor ganglion at late tailbud I (St.23). (D) Representative time-course images of Ca^{2+} oscillation at St.23. A10.64 is labeled with Kaede-NLS (white arrowhead). Ca^{2+} oscillation overlapped with the nuclear signal from Kaede-NLS (yellow arrowhead). Enlarged views of A10.64 are embedded in each panel (inset). N=6.

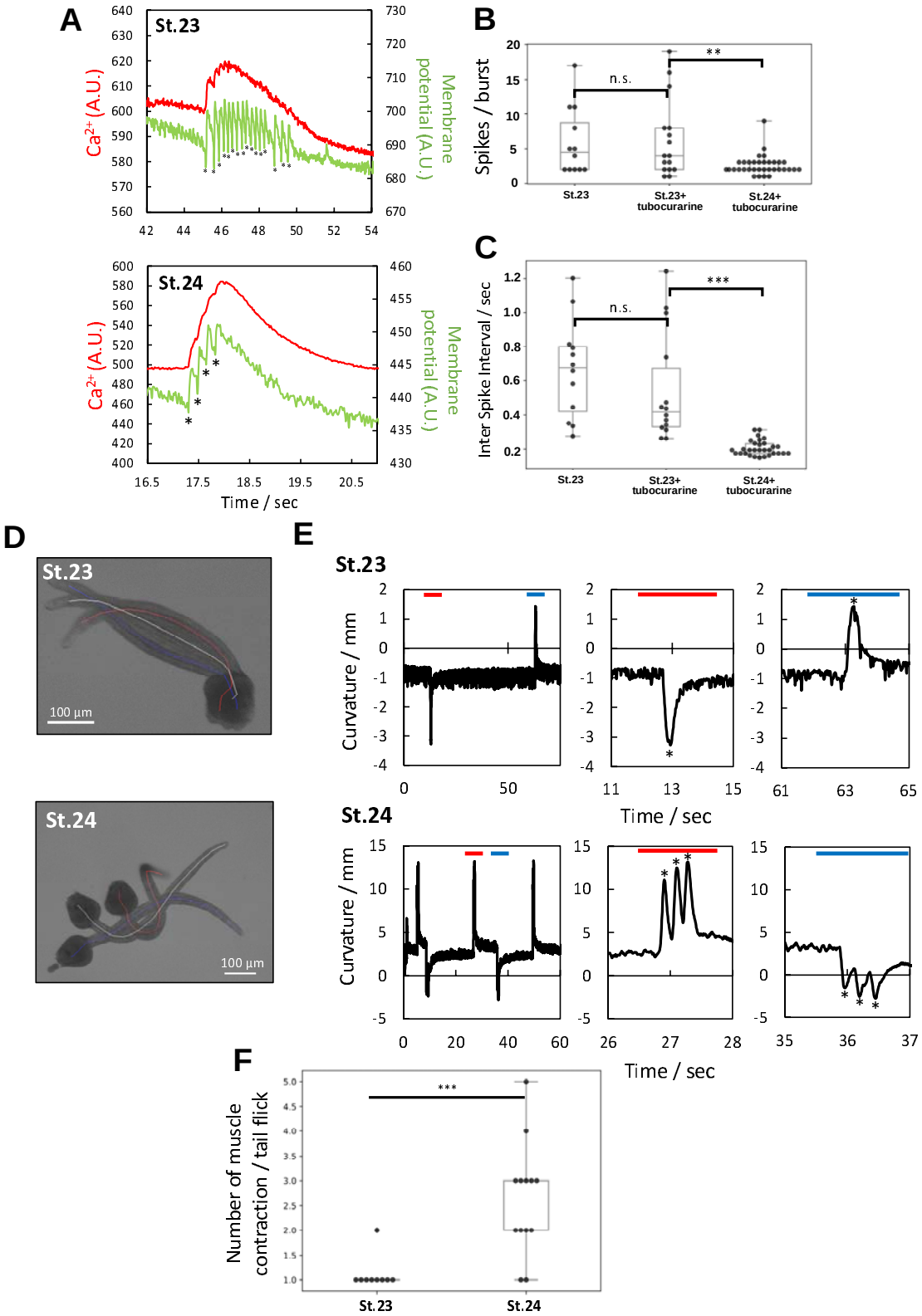

Figure 3. Muscle contraction couples with the neuronal activity of A10.64.
(A) Representative fluorescence intensity of Ca^{2+} (red) and membrane potential (green) in A10.64 at St.23 (top panel) and St.24 (lower panel). The fluorescence intensity of ASAP2f decreases upon depolarization (26). Asterisks indicate the timing of depolarization. (B) Box plot of numbers of spikes in bursts in A10.64. Data are presented as means ± S.D. (n = 7, 12, and 11 for tubocurarine 0 mM (St.23), 5 mM (St.23), and 5 mM (St.24), respectively; ** P<0.05; Wilcoxon rank–sum test). (C) Box plot of inter-spike intervals in A10.64. Data are presented as means ± S.D. (n = 7, 11, and 11 for tubocurarine 0 mM (St.23), 5 mM (St.23), and 5 mM (St.24), respectively; ** P<0.05; Wilcoxon rank–sum test). (D) Three merged images of late tailbud I (St.23, upper panel) and late tailbud II (St.24 lower panel), captured by a high-speed camera. The midlines of the embryos are indicated in white (resting state), red (the timing of right muscle contraction), and blue (the timing of left muscle contraction). (E) The time course of the curvature calculated from the midline at late tailbud I (St.23, upper panel) and late tailbud II (St.24 lower panel). Red and blue bars indicate representative right and left muscle contractions, respectively. Magnified time course of curvature at red and blue bars is indicated in the right graphs, respectively. Asterisks indicate the timing of tail muscle contraction. (F) Box plot of the number of muscle contractions in one ETF at St.23 and St.24. Data are presented as means ± S.D. [n = 9 (St.23) and 13 (St.24) from 3 and 2 embryos respectively; *** P<0.01; Wilcoxon rank–sum test].

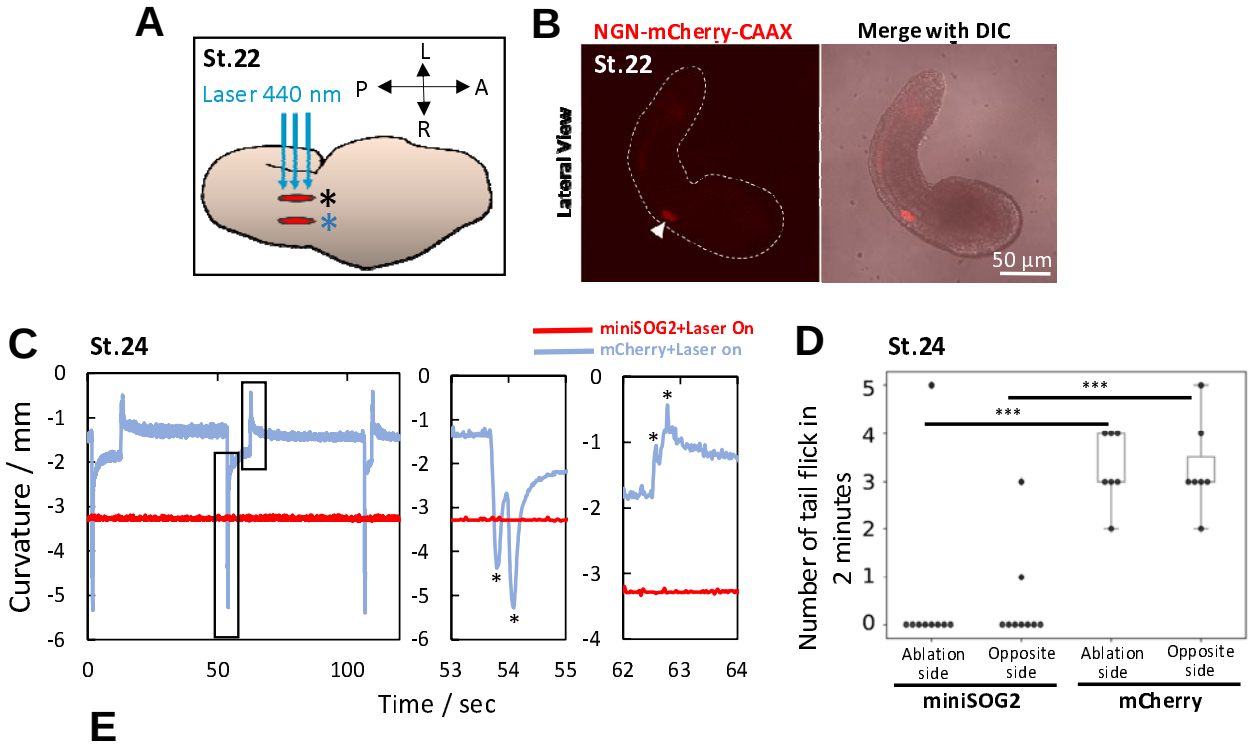

Figure 4. Single-cell photoablation for A10.64 abrogates the ETF until St.24.
(A) Schematic illustrations of the scheme for photoablation of A10.64. A10.64 cells are illustrated in red. A 440-nm laser was applied from the lateral side. The upper and lower sides of A10.64 are marked by black and blue asterisks, respectively. (B) Fluorescence image (left) and merged image with DIC (right) at mid tailbud II (St.22) in an embryo electroporated with Neurog::mCherry-CAAX. The signal of mCherry-CAAX in A10.64 is indicated by a white arrowhead. (C) Time course of the curvature, calculated from the midline, for 120 sec. Blue line indicates the curvature of embryos electroporated with Neurog::mCherry-CAAX (for control). Red line indicates the curvature of embryos electroporated with Neurog::minisog2-CAAX and Neurog::mCherry-CAAX. Magnified time course of curvature (black rectangles) is indicated in the right graphs. (D) The number of ETFs in 2 min at St.24 under each condition. The upper side of A10.64 (Fig. 5A, black asterisk) is indicated as the “Ablation side”. The lower side of A10.64 (Fig. 5A, blue asterisk) is indicated as the “Opposite side”. Data are presented as means ± S.D. [N = 9 (electroplated with Neurog::minisog2-CAAX and Neurog::mCherry-CAAX) and 7 (electroplated with mCherry-CAAX, for control); *** P<0.01; Wilcoxon rank–sum test]. (E) The summary of the Ca^{2+} oscillation and membrane potential in A10.64 and its relationship to the early spontaneous motor behavior from St.22 to St.24. Neural tubes (blue), muscle (red), A10.64 (green), and neuromuscular junction (NMJ, yellow) are indicated by black arrows. The asterisks and curved arrow indicate the number of muscle contractions in one Ca^{2+} oscillation or ETF.

Supporting information

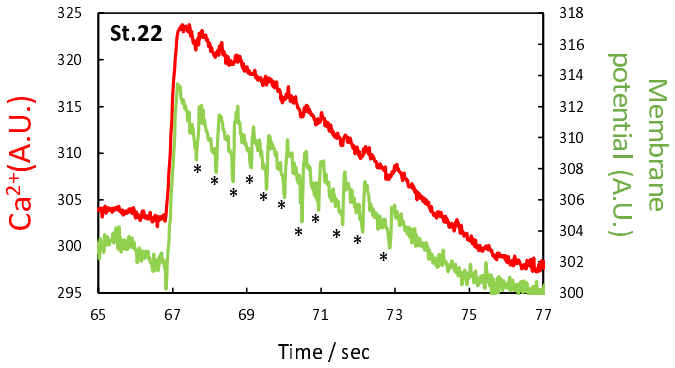

Suppl. Figure 1. The representative fluorescence intensity of Ca^{2+} and membrane potential in A10.64 at St.22.

Fluorescence intensity of Ca^{2+} and membrane potential are indicated in red and green, respectively. The fluorescence intensity of ASAP2f decreases by depolarization (26). Asterisks indicate the timing of depolarization.

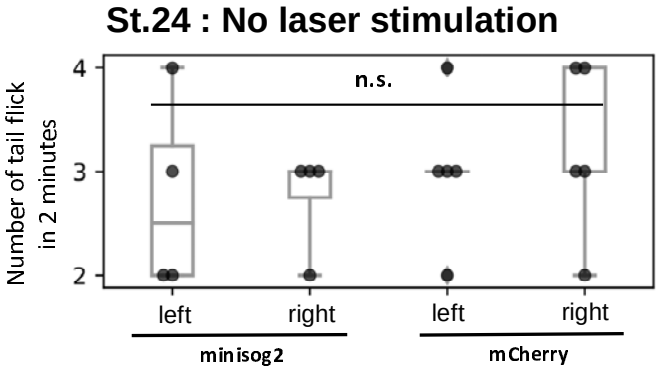

Suppl. Figure 2. Observed number of ETFs in 2 min at St.24 under each condition.

Embryos were electroporated with Neurog::minisog2-CAAX and Neurog::mCherry-CAAX (indicated as minisog2), or Neurog::mCherry-CAAX (indicated as mCherry). No laser stimulation was applied to A10.64 under any condition. Data are presented as means ± S.D. [N = 4 (electroplated with Neurog::minisog2-CAAX and Neurog::mCherry-CAAX) and N = 5 (electroplated with mCherry-CAAX, for control); n.s., not significant; Wilcoxon rank–sum test].

Suppl. Movie 1. Whole-body Ca^{2+} imaging using GCaMP6s at mid tailbud II (St.22).

Fluorescence imaging of mid tailbud II (St.22) expressing GCaMP6s. Ca^{2+} oscillation was observed in the motor ganglion. The other Ca^{2+} transients observed in this video were derived from epidermis (20), and did not couple with the Ca^{2+} oscillation in the motor ganglion. Time-lapse imaging was recorded from the lateral side.

Suppl. Movie 2. Whole-body Ca^{2+} imaging using H2B-GCaMP6s at mid tailbud II (St.22).

Fluorescence imaging of mid tailbud II (St.22) expressing H2B-GCaMP6s, recorded by confocal laser-scanning microscopy. Ca^{2+} oscillation was observed only in a single nucleus in the motor ganglion. The other Ca^{2+} transients observed in this video were derived from epidermis (20), and did not couple with the Ca^{2+} oscillation in the motor ganglion. The time-lapse images were recorded from the lateral side.

Suppl. Movie 3. Dissociated single-cell Ca^{2+} oscillation.

Imaging of the dissociated single cells expressing GCaMP6s was recorded by fluorescence microscopy. The time-lapse image was recorded at 1-sec intervals.

Suppl. Movie 4. Long time-lapse Ca^{2+} imaging using GCaMP6s, from mid tailbud II (St.22) to late tailbud II (St.24).

Fluorescence imaging of embryos expressing GCaMP6s. After about 7 min, the Ca^{2+} elevation in the tail muscle gradually came to coincide with the ipsilateral tail muscle contraction. The Ca^{2+} transients derived from epidermis were also observed in this video (20).

Suppl. Movie 5. Simultaneous imaging of Neurog::Kaede-NLS and pSP-CiVACHT::GCAMP6s at late tailbud I (St.23).

Simultaneous imaging of Neurog::Kaede-NLS and pSP-CiVACHT::GCAMP6s at late tailbud I (St.23), recorded by confocal laser-scanning microscopy. A10.64 labeled with Kaede-NLS showed Ca^{2+} oscillation. The time-lapse image was recorded from the lateral side.

Suppl. Movie 6. Bright-field recording of a hatched larva (St.26) in which A10.64 was laser-ablated at St.22.

In the hatched larva (St.26) shown in this video, A10.64 was ablated at St.22. The embryo did not exhibit early spontaneous motor behavior at St.24 (Fig. 4C, red lines). Muscle contraction occurred frequently at St.26, although normal swimming behavior was not observed.